Phase-Based Level Set Segmentation of Ultrasound Images

Ahror Belaid, Djamal Boukerroui, Y. Maingourd, and Jean-Francois Lerallut, *Senior Member, IEEE*

***Abstract*—Ultrasonic image segmentation is a difficult problem due to speckle noise, low contrast, and local changes of intensity. Intensity-based methods do not perform particularly well on ultrasound images. However, it has been previously shown that these images respond well to local phase-based methods which are theoretically intensity invariant. Here, we use level set propagation to capture the left ventricle boundaries. The proposed approach uses a new speed term based on local phase and local orientation derived from the monogenic signal, which makes the algorithm robust to attenuation artifact. Furthermore, we use Cauchy kernels, as a better alternative to the commonly used log-Gabor, as pair of quadrature filters for the feature extraction. Results on synthetic and natural data show that the proposed method can robustly handle noise, and captures well the low contrast boundaries.**

***Index Terms*—Echocardiography, level set, local phase, monogenic signal, segmentation.**

I. Introduction

ULTRASOUND imaging is an exploration technique commonly used in many diagnostic and therapeutic applications. It has many advantages: it is noninvasive, provides images in real time, and requires lightweight material. However, ultrasound B-scan images are known to have low signal-to-noise ratio, low contrast, and high amounts of speckle [1]. This image texture, or speckle, is a correlated and multiplicative noise that inherently occurs in all types of coherent imaging systems. Hence, it makes modeling difficult as its statistics depend on the density and on the type of scatterers in the tissues [1]–[6]. All these characteristics make segmentation difficult, and therefore, complicate the diagnosis task.

A correct segmentation of structures is crucial in many medical applications. In clinical practice, the quantification of these structures is generally performed by manual tracing, which is a time consuming and by the application of geometrical assumptions that could introduce measurement errors in presence of pathologies. Hence, reliable, rapid, accurate, and automatic or semiautomatic methods of structures extraction are required. Fully automatic segmentation of ultrasound images still remains a challenging topic [7].

Several approaches have been reported in the literature for automated or semiautomated border detection from ultrasound images. For instance, statistical models, arguing that these were more appropriate because of the significant noise and missing boundaries of ultrasound images, have been extensively used [7], [8]. For this reason, several probability density functions were used to model image gray levels statistics [9]–[18]. Probably, all exiting modeling paradigms and segmentation approaches have been tried on ultrasound data. A comprehensive recent survey is given in Noble and Boukerroui [7]. Recent works suggests that there is an increase of interest on statistical modeling of both uncompressed and compressed envelope of the backscattered signal, [8], and their use in level set segmentation algorithm [14], [16], [19]–[21]. Shape and time information are also of a great interest in a number of applications [16].

In this study, we refer to echocardiographic data. It is known that echocardiography has been one of the driving application areas of medical ultrasound and the literature on methods for automatically segmenting and tracking the left ventricle is extensive. As it has been pointed in [7], the most popular approach has been to treat echocardiographic endocardial segmentation as a contour finding approach. This is not straightforward as the contrast around the left ventricle chamber boundaries varies, depending on its relative orientation to the transducer direction, and to attenuation. Thus, conventional intensity gradient-based methods have had limited success on typical clinical images. To avoid this drawback, phase-based approach offers a good alternative, since it makes the approach robust to attenuation artifacts. It is within this framework that we propose an alternative in this paper.

A model of feature perception called the local energy model has been developed by Morrone *et al.* [22], [23]. This model postulates that features are perceived at points in an image, where the Fourier components are maximally in phase. A wide range of feature types give rise to points of high-phase congruency. These include step edges, line and roof edges, and Mach bands. It has been shown that this model successfully explains a number of psychophysical effects in human feature perception. Other important work on this model of feature perception can be found in [24]. Mulet-Parada and Noble [25], [26] were the first to successfully use the local phase information for boundary detection on echocardiographic images.

Some phase-based level set methods on segmentation [27]–[29], image enhancement [30], and registration [31], [32]

Manuscript received April 8, 2010; revised September 22, 2010; accepted October 25, 2010; Date of publication November 9, 2010; date of current version January 4, 2011. This work was supported by a grant of the Regional Council of Picardie and European Union/FEDER.

A. Belaid, D. Boukerroui and J.-F. Lerallut are with Heudiasyc UMR CNRS 6599, Université de Technologie de Compiègne, Centre de Recherche de Royallieu, 60205 Compiègne Cedex, France (e-mail: ahror.belaid@hds.utc.fr, djamal.boukerroui@hds.utc.fr, jean-francois.lerallut@hds.utc.fr).

Y. Maingourd is with the Pediatric Échocardiographic Center, Centre Hospitalier Universitaire Amiens, Amiens 80054, France (e-mail: maingourd.yves@chu-amiens.fr).

Color versions of one or more of the figures in this paper are available online at http://ieeexplore.ieee.org.

Digital Object Identifier 10.1109/TITB.2010.2090889

on medical applications can be found in the literature. There is also a great increase of AM–FM methods and their use in medical applications [33], [34]. Also, phase information has been used in numerous applications, such as segmentation [35], wavelets [36] and AM–FM [35], [37], [38] image analysis, stereo matching [39], [40], optical flow [41], denoising [42], and corner and edge detection [24], [43]–[46]. Phase-based processing has attracted a lot of attention in image analysis, but probably not still enough in ultrasound image segmentation [7].

This paper concerns the development of a novel segmentation method of the left ventricle within the level set framework. This uses local phase information derived from the monogenic signal, which is a multidimensional extension of the analytic signal [44]–[46]. Our idea is to use a novel speed function, which combines the local phase and local orientation in order to detect boundaries in low contrast regions. A preliminary results of this work appeared in [47].

In the next section, we describe the extraction of local properties (phase, orientation, and amplitude) from 1-D and 2-D signals. The proposed segmentation method is presented in Section III. Section IV shows qualitative and quantitative experimental results on both synthetic and natural data. Section V provides a discussion followed by some concluding remarks in Section VI.

II. Background

Openheimer and Lim [48] showed that when using two synthetic images, one of them containing only the phase information while setting its amplitude information to unity, and the other containing only the amplitude information while the phase is set to zero, only the image containing the phase is visible, although deteriorated. The image containing amplitude information is completely indiscernible. The information carried by the phase of a picture appears to be much more significant than the information carried by its amplitude. Indeed, the phase informs us about the location and orientation of image features, while the amplitude provides only information on their intensity. One of the popular methods to estimate local signal information is based on the analytic representation of the signal. Details for 1-D and *n*-D signals are given in the subsequent sections.

A. Monogenic Signal

To extract the local properties (amplitude and phase) of a 1-D signal $f(x)$, we need to represent it in its analytic form as presented in [49, Ch. 4]

$$f_A(x) = f(x) - if_{\mathcal{H}}(x)$$

where $i = \sqrt{-1}$ and $f_{\mathcal{H}}(x)$ is the Hilbert transform of $f(x)$. The local amplitude (energy) and local phase of $f(x)$ are given by

$$A(x) = \|f_A(x)\| = \sqrt{f^2(x) + f^2_{\mathcal{H}}(x)},$$
$$\varphi(x) = a\tan2(f_{\mathcal{H}}(x), f(x)).$$

Recently, Felsberg and Sommer [45], [46], proposed a novel *n*-D generalization of the analytic signal based on the Riesz transform, which is used instead of the Hilbert transform. Also, they proposed a 2-D isotropic analytic signal, called *monogenic signal*. This representation preserves the core properties of the 1-D analytic signal that decomposes a signal into information about structure (local phase) and energy (local amplitude). Felsberg and Sommer introduced the following filters in the frequency domain [44]:

$$H_1(u_1, u_2) = i\frac{u_1}{\sqrt{u_1^2 + u_2^2}}$$
$$H_2(u_1, u_2) = i\frac{u_2}{\sqrt{u_1^2 + u_2^2}}.$$

The spatial representation of the earlier filters is given by

$$h_1(x_1, x_2) = \frac{-x_1}{2\pi(x_1^2 + x_2^2)^{3/2}}$$
$$h_2(x_1, x_2) = \frac{-x_2}{2\pi(x_1^2 + x_2^2)^{3/2}}.$$

The monogenic signal $\mathbf{f}_M$ is then defined as a 3-D vector formed by the signal $f(x_1, x_2)$ with its Riesz transform $\mathbf{f}_{\mathcal{R}} = (\mathbf{h} * f)(x_1, x_2)$, with $\mathbf{h} = (h_1, h_2)$, by

$$\mathbf{f}_M(x_1, x_2) = (f, \mathbf{h} * f)(x_1, x_2) \quad (1)$$
$$= (f, \mathbf{f}_{\mathcal{R}})(x_1, x_2). \quad (2)$$

In the *n*-D case, the local phase is associated to a given local orientation due to the fact that structural information is related to a given orientation. The concept of *local phase vector* is proposed by Felsberg and Sommer [45], [46] and is defined by

$$\Phi = \varphi \cdot \mathbf{r} \quad (3)$$
$$\Phi = a\tan\left(\frac{\|\mathbf{f}_{\mathcal{R}}\|}{f}\right)\frac{\mathbf{f}_{\mathcal{R}}}{\|\mathbf{f}_{\mathcal{R}}\|} \quad (4)$$

where $a\tan(\cdot) \in [0, \pi]$. The *monogenic phase* Φ (*local phase vector*), is similar to the product of 1-D local phase φ, multiplied by the orientation vector $\mathbf{r}$, if the underlying signal is $i1$-D (intrinsically 1-D signals). The defined local phase vector can be interpreted as a rotation vector, which magnitude corresponds to the phase angle between the real signal and the monogenic signal, (see Fig. 1). In contrast to the 1-D case, the phase now includes additional geometric information. The monogenic phase completely characterizes the local gray-level transition of an image (i.e., local structure) as long as the image is locally $i1$-D, given that the phase has been defined with respect to a given orientation. The phase vector orientation $\mathbf{r}$ represents the local orientation of the image and is defined by the following relation [44]:

$$\theta = a\tan\left(\frac{h_2 * f}{h_1 * f}\right). \quad (5)$$

B. Quadrature Filters

In practical applications, the local properties are estimated using a pair of bandpass quadrature filters. Indeed, the detection of local properties by the monogenic signal assumes that the signal consists of few frequencies that is bandlimited. A real

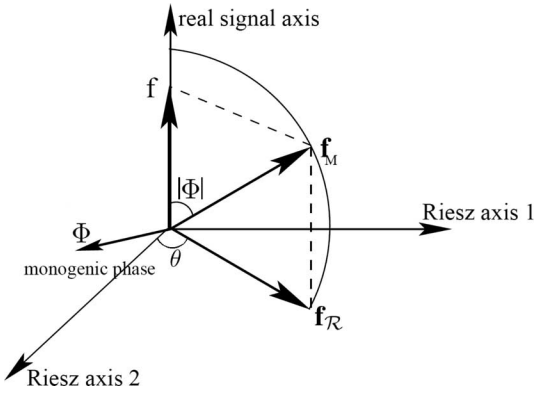

Fig. 1. Monogenic phase represented by means of a rotation vector. The amplitude of the rotation vector is the angle between the real and the monogenic signals. The rotation vector is orthogonal to the plane spanned by the real-signal axis and $\mathbf{f}_\mathcal{R}$.

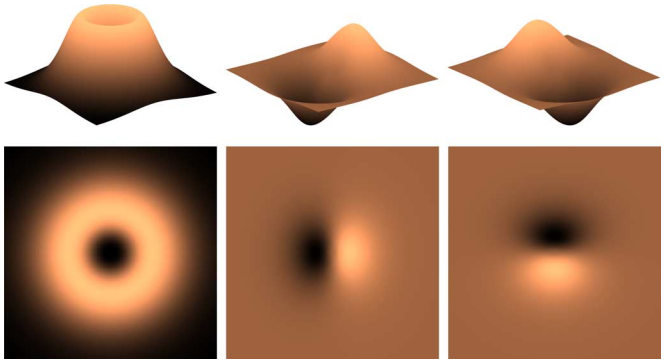

Fig. 2. 2-D Cauchy kernels in Fourier domain for a certain parameter $s > 0$. From left to right: isotropic even, and the pair of odd filters.

image consist of a wide range of frequencies, therefore a set of bandpass filters needs to be combined with the monogenic signal. Equations (1) and (2) become

$$\mathbf{f}_M(x_1, x_2; s) = (c * f, c * \mathbf{h} * f)(x_1, x_2) \tag{6}$$

$$= (c * f, c * \mathbf{f}_\mathcal{R})(x_1, x_2) \tag{7}$$

where $c(x_1, x_2; s)$ is the spatial domain representation of an isotropic bandpass filter and $s > 0$ is a scaling parameter. Thus, the monogenic signal can be represented by a scalar-valued even and vector-valued odd filtered responses, with the following simple tick:

$$\text{even} = c * f$$

$$\mathbf{odd} = (c * h_1 * f, c * h_2 * f).$$

Several families of quadrature pairs have been proposed and applied in the literature. Most authors have not provided a reasonable justification for the use of a particular family apart from simplicity of use or the satisfaction of the zero dc condition. In [50], [51], Boukerroui *et al.* compare several 1-D pairs of quadrature filters and concluded that log-Gabor kernels are probably not a very good choice in the case of feature detection. They showed that Cauchy family has better properties (see Fig. 2). In the frequency domain, a 2-D isotropic Cauchy kernel is defined by

$$C(\mathbf{u}) = n_c |\mathbf{u}|^a \exp(-s|\mathbf{u}|), \quad a \geq 1 \tag{8}$$

where $\mathbf{u} = (u_1, u_2)$, s is a scaling parameter, and a/s is the peak tuning frequency of the filter. n_c is a normalization constant, see [50], [51] for more details.

In this paper, a Cauchy kernel is used as a bandpass filter. Interestingly, Cauchy filter could be seen as the a^{th} spatial derivative of the Poisson filter,[1] given in the frequency domain by

$$P(\mathbf{u}) = \exp(-2\pi|\mathbf{u}|s)$$

introduced in [46]. The authors have proved that the Poisson kernel establishes a linear and isotropic scale space: *the Poisson scale space*. The main property of this new scale space is its close relation to the monogenic signal. Hence, local phase and local amplitude, becomes inherent features of scale-space theory.

C. Edge Detection Measure

Step edge detection is performed using the *feature asymmetry* measure (FA) of Kovesi [24] defined using the monogenic signal presented previously. To identify step edges essentially involves finding points, where the absolute value of the local phase is 0° at a positive edge and 180° at a negative edge. In other words, the difference between the odd and the even filter responses is large. Kovesi suggested to use FA over a number of scales to detect step edge features. We define the multiple scales feature asymmetry

$$\text{FA} = \sum_s \frac{\lfloor |\mathbf{odd}_s| - |\text{even}_s| - T_s \rfloor}{\sqrt{\text{even}_s^2 + \mathbf{odd}_s^2} + \varepsilon} \tag{9}$$

where $\lfloor \cdot \rfloor$ denotes zeroing of negative values and T_s is the scale specific noise threshold [24]. The FA takes values in $[0, 1]$, close to zero in smooth regions and close to one near boundaries.

The application of this operator in [25] and [30] for ultrasound images has yielded good results. The authors used FA with steerable filter for boundary detection. However, it is expected to obtain better results using the monogenic signal, as it is the natural extension of the 1-D analytical signal.

III. Description of the Model

In this section, we present our proposed segmentation method. The idea is to use a novel-phase-based speed function within the level set framework.

Consider a gray level image as a function $I : \Omega \to \mathbb{R}^+$, where $\Omega \in \mathbb{R}^2$ is the image domain. The image gradient vector field is given by $\nabla I(x, y)$. Let us define the evolving contour $C : [0, L] \to \mathbb{R}^2$, given in a parametric form $C(p) = \{x(p), y(p)\}$, where p is an arclength parameter, and whose normal is defined by $\mathbf{n}(p) = \{-y_p(p), x_p(p)\}$.

The alignment term idea proposed by Kimmel *et al.* [52], is to search for a contour C that interacts with a given image, such

[1]Here, the derivative is taken in the spatial domain in the radial direction, which preserves the isotropy property in higher dimension.

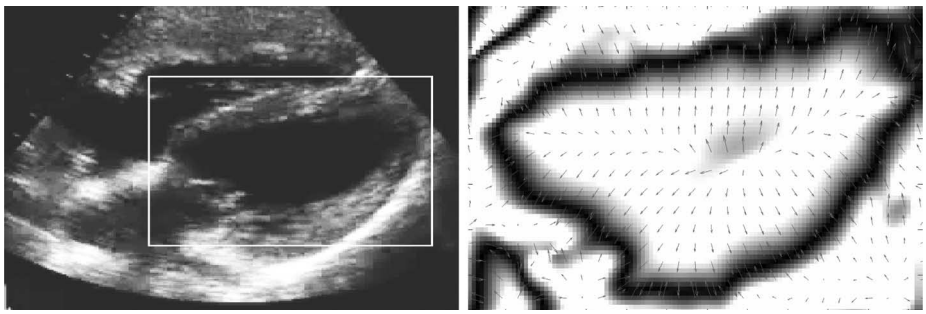

Fig. 3. (Left) Original echocardiographic image of a four chamber view with a defined region of interest (ROI). (Right) Underlying gray value image shows the g function given in (12) and the vector field show the local phase vector field, both calculated on the showed ROI.

that the curve's normal aligns with the gradient vector field.The alignment of the two vectors can be measured by their inner product that we denote by $\langle \mathbf{n}, \nabla I \rangle$. The geometric functional of the alignment measure in its robust form is given by [52], [53]

$$E_A(C) = -\int_0^L |\langle \mathbf{n}(p), \mathbf{V}(x(p), y(p)) \rangle| dp \qquad (10)$$

where $\mathbf{V}$ is a given vector field (e.g., image gradient). The functional $E_A(C)$ measures the alignment between the local image orientations and the curve's normals. In the proposed work, we use the local orientation computed by means of the monogenic phase Φ given by (4) instead of the classical gradient estimation. As shown in Fig. 3, the monogenic phase offers a good orientation estimation of the edge. The inner product $\langle \cdot, \cdot \rangle$ gets high values if the curve's normals align with the local orientations of the image. This is useful in low contrast boundaries.

In our active contour model, we will minimize the earlier alignment term and we will add some regularizing terms. It is known in literature that when we use several terms, geodesic active contour model (GAC) [54] serves as a good regularization for other dominant terms. Therefore, we introduce the following energy functional to be minimized:

$$E(C) = -\int_0^L |\langle \mathbf{n}(p), \mathbf{V}(x(p), y(p)) \rangle| dp + \lambda \int_0^L g(C(p)) dp + \nu \int\int_{\Omega_C} g(x, y) dx dy. \qquad (11)$$

The second term is the GAC term, where g is an inverse edge indicator function, generally taken as $g(x, y) = 1/(1 + |\nabla G_\sigma * I|)$, and the integral is computed along the contour. Here, G_σ is the Gaussian kernel with standard deviation σ. The search in this case, would be for a curve along which the inverse edge indicator gets the smallest possible values. Thus, the values of g are close to one in smooth regions and close to zero near boundaries. The third term is a weighted region term as in [54]. It measures the area inside the curve C, i.e., the area of the region Ω_C.

In this paper, we define and use a phase-based edge indicator function instead of the classical inverse gradient based one, by the following new formulation:

$$g = 1 - (FA)^\alpha \qquad (12)$$

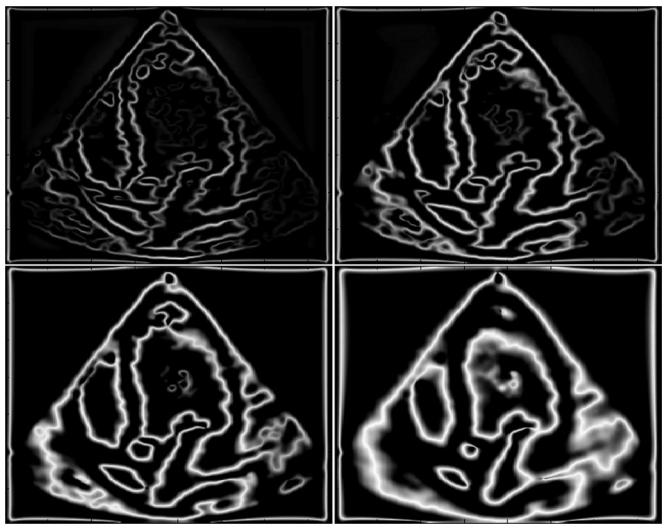

Fig. 4. Examples of feature asymmetry measure at different scales. From top-left to bottom-right: $s \in \{15, 20, 25, 30\}$, filters bandwidth $= 2.5$ octaves, i.e., $a = 1.92$ (see [50]). The original image can be seen in Fig. 6 (left).

where $\alpha \in [0, 1]$ is a hyperparameter and FA $\in [0, 1]$ is the feature asymmetry measure, defined by (9). As it was mentioned in Section I, a recent works showed that ultrasound images respond well to phase-based edge detection. Moreover, a multiscales approach offers a better control on the edge detection quality. As shown in Fig. 4, by moving closer to finer scales, the FA measure recovers details and discontinuities, but looses regularity and continuity of the boundaries.

We embed a closed curve in a higher dimensional $\phi(x, y)$ function, which implicitly represents the curve C as a zero set, i.e., $C = \{\{x, y\} : \phi(x, y) = 0\}$. Following [53], the gradient descent flow minimizing (11), in the level set formulation, is given by

$$\frac{\partial \phi}{\partial t} = \Bigg[-\mu \text{sign}(\langle \Phi, \nabla \phi \rangle) \text{div}(\Phi) + \lambda \text{div}\left(g(x, y) \frac{\nabla \phi}{|\nabla \phi|} \right) + \nu g(x, y) \Bigg] |\nabla \phi| \qquad (13)$$

where μ, λ, and ν are positives fixed parameters. The sign function in the first term can be simplified and written as $\text{sign}(\nabla_{\mathbf{r}} \phi)$, where $\nabla_{\mathbf{r}}$ is a gradient operator in the direction specified by $\mathbf{r}$, (see Appendix).

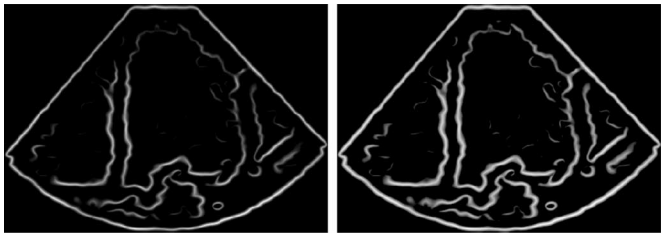

Fig. 5. Influence of the parameter α on the edge detection quality using the FA measure. (Left) $\alpha = 1$ and (right) $\alpha = 0.5$. The original image is given on Fig. 6 (right).

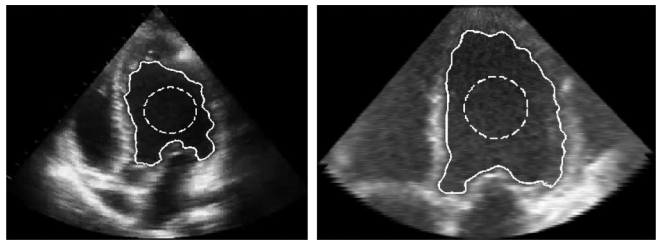

Fig. 6. Example of phase-based level set segmentation results of the left ventricle. The inner contours are the respective initializations.

IV. Experimental Results

MATLAB 7.6 (R2008a) was used for the implementation of the proposed method. Our program required approximately 15 s of CPU time per image (image size 256×256) on an IBM Intel Xeon single-CPU 3.4 GHz. In most of the experimental results shown in this section, the following parameters were fixed as such: bandwidth $= 2.5$ octaves as suggested in [50], wavelength $= 20$ pixels for natural data, and 10 pixels for synthetic data. These settings were roughly consistent with the ones used by Mulet-Parada and Noble [26]. We found by experiment that large α value would cause leakage of the endocardial contour. We therefore chose the largest α that did not have a leakage problem (see Fig. 5). In practice, we set $\alpha = 0.5$.

The GAC parameter λ is not set to the same value in all experiments. If we have to detect many objects of different sizes, then λ should be small. Conversely, if we have to detect only large objects, and to not detect smaller objects, then λ has to be larger. We also found by experiment that $\nu = 0.1$ was appropriate for most datasets.

The proposed variational level set method has been applied to a variety of natural and synthetic images. We compared the results of our approach with those of two other closely related algorithms. The first is the gradient-based version of our approach, which is the GAC presented in [54]. This algorithm has the same data adherence terms as our approach, but it lacks the alignment term. As suggested by Kimmel [55] for noisy images, the alignment term is turned off. The second algorithm (GAC + ML) is an alternative of the first one in which we strengthen it by a region-based term as presented in [14]. This model evolves according to image information using image gradient and an *a priori* knowledge about the statistical distribution of image gray levels. Specifically, the observed image gray levels are modeled by a Rayleigh distribution. The region-based term drives the curve evolution to achieve a *maximum likelihood* segmentation of the target, with respect to the statistical distribution law of image pixels.

Fig. 4 shows the edge detection function applied on real ultrasound image. It is computed by the FA measure, using the monogenic signal with the Cauchy filters. By moving closer to the coarse scales, edge detection looses details but recovers regularity of the boundaries. As shown in the top left of Fig. 4, finer scales do not detect weak boundaries, and may lead to segmentation leakages. Notice that the edges regularity can be controlled by the filter scaling parameter s and the GAC parameter λ. This is the reason why we have fixed the value of the scaling parameter and preferred adjusting the value of the GAC parameter in order to compare with similar approaches.

Fig. 6 shows illustrative results of our method on two typical ultrasound images (left ventricle). Fig. 7 shows illustrative comparison results of the proposed phase-based level set (PBLS) segmentation algorithm with the results of the GAC and the GAC + ML algorithms. These results give the reader some insight regarding the robustness to speckle noise and to attenuation.

In order to evaluate the proposed method and quantify its accuracy, we have used a set of manually delineated contours. We have collected a set of 20 bidimensional cardiac ultrasound images, obtained from a Philips IE33 echocardiographic imaging system. The dataset was segmented by two specialists in an independent way, i.e., in different days, at the Pediatric Echocardiographic Center, CHU Amiens. Each specialist segments each image five times, so that ten manual segmentations are available for each image. Thus, in all, we have 200 manual segmentations. This allows measuring the inter- and intraobserver variabilities, which are the differences performed by the same specialist as well as the differences between segmentations performed by different specialists, respectively.

Two distances have been used to compute the comparison between two contours. The first distance, referred here to as *dice similarity coefficient* (DSC), is given by [56]

$$\mathrm{DSC}(S_1, S_2) = 2\frac{|S_1 \bigcap S_2|}{|S_1| + |S_2|} \tag{14}$$

where S_1 and S_2 represent the ground truth and the obtained segmentation, and $|.|$ denotes the cardinal of a set. The closer the DSC values to 1, the better is the segmentation. The second measure is the distance between two given curves, C_1 and C_2 represented as sets of ordered pairs of the x and y coordinates of points $C_1 = \{a_1, a_2, \ldots, a_n\}$ and $C_2 = \{b_1, b_2, \ldots, b_m\}$. The distance between the point a_i and the closest point on the curve C_2 is computed by

$$d(a_i, C_2) = \min_{b_j \in C_2} \|b_j - a_i\|.$$

These distances are computed for all points of the two curves and are averaged to yield the *mean absolute distance* between

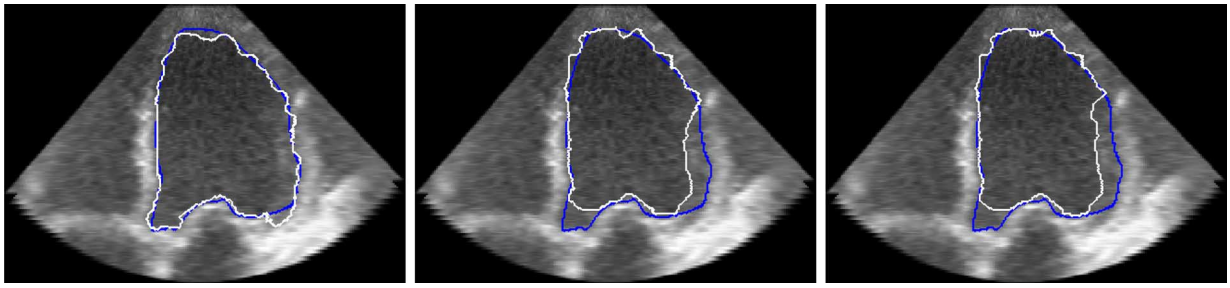

Fig. 7. Comparison of the PBLS (left), GAC (middle), and GAC+ML (right) results with a manual delineation. Blue line indicates manual delineation, and white line indicates semiautomatic segmentation.

TABLE I
PERFORMANCE INDICES MEASURES DSC (%) AND MAD (PIXELS) VERSUS INTRAOBSERVER, INTEROBSERVER, AND COMPUTER-OBSERVER DISTANCES

Measures	DSC (%)			MAD		
Indexes	Mean	Median	SD	Mean	Median	SD
GAC	84.87	88.43	9.42	7.47	5.81	4.05
GAC+ML	86.78	89.08	8.85	6.61	5.19	4.32
PBLS	89.91	91.88	6.01	5.59	4.33	3.33
Intraobserver	96.15	96.51	0.92	2.39	2.20	0.65
Interobserver	93.66	93.82	3.67	3.80	3.06	2.48

Mean, median and standard deviation for DSC and MAD are shown.

the two curves $\mathrm{MAD}(C_1, C_2)$ [57]. Hence,

$$\mathrm{MAD}(C_1, C_2) = \frac{1}{2}\left[\frac{1}{n}\sum_{i=1}^{n} d(a_i, C_2) + \frac{1}{m}\sum_{i=1}^{m} d(b_i, C_1)\right]. \tag{15}$$

Table I shows a quantitative comparison between the three semiautomatic segmentation: our approach—that we denote in what follow PBLS for phase-based level set—, GAC, GAC + ML, and manual segmentation (intraobserver and interobserver) for the 20 echocardiographic images. The mean, median, and standard deviation of the 20 results are shown for both measures (see Fig. 8).

The first result is the segmentation performed by the classical-gradient-based GAC, the second one is the segmentation using GAC with the ML region term (see [14]) and the third one is the segmentation using our PBLS (11).

We have also used the simulation program Field II [58], [59], to synthesize phantom data with known ground truth. The phantom consists of 100 000 scatterers, and simulating 50 radio frequency lines. It consists of four columns with different contrasts, each one contains three circles with different scales (17, 20, and 23 pixels radius), see Fig. 10.

The segmentation results obtained by the GAC, GAC + ML model, and the proposed method are shown in Fig. 11. The results were obtained with $\lambda = 0.1$ for the GAC method and $\lambda = 0.6$ for PBLS and GAC + ML methods. Fig. 12 summaries the quantitative evaluations of the three segmentation models on this dataset.

V. DISCUSSION

The quantitative evaluation on the natural data (see Tables I and II) show, as expected, that the use of GAC with an additional region term provides a significant improvement with respect to the classical GAC. This is due to the fact that solely edge detection technique does not work for echocardiographic images with weak edges. The region term also improves the edge detection by avoiding local minima of the energy function, as a simple gradient descent is used. See, e.g., [19], [20] for an alternative minimization.

Now observe that the use of PBLS improves even more the already good results of the GAC + ML. Indeed, one of the major problems encountered in applying region-based method on ultrasound images, is the attenuation. In highly corrupted images with local intensity variations, the region term cannot segment the blood part of the left ventricle as a single region. Undoubtedly, the underlying assumption of a single tissue with Rayleigh statistics is not valid in such situations. The proposed phase-based term is more robust to attenuation artifact for being theoretically intensity invariant. It should also be remembered that in our approach, the phase-based GAC term is reinforced by the phase-based alignment term.

The intraobserver values are the mean of the values of DSC (%) and MAD after comparing all the manual segmentations of each specialist for each image. Interobserver values are the mean of the comparisons performed by different specialists. The interobserver results show that there is a significant difference between the segmentation of the two specialists (see details in Table II). As expected, the intraobserver differences are lower than the interobserver ones, and the later are less than all the semiautomatic ones (GAC, GAC + ML, and PBLS). The low variances of the intraobserver for both measures suggest a regularity of the segmentations of two specialists. This is confirmed by the details shown in Table II and the graphics shown in Fig. 8. Indeed, Fig. 8 shows separately the quality of segmentation associated to the specialists. In the same table and figure, we can detect images with low contrast and high speckle noise, which are difficult to segment by both physicians. For instance, image number 19 is difficult to segment, as it is suggested by the low mean and high standard deviation of the DSC measures for both physicians.

Table I suggests that the PBLS segmentations are not as good as the manual ones, but still very close to the ground truth. It can be observed, in Fig. 9, that the manual results are more regular, while the automatic results have more details. Note that our quantitative evaluation is similar to the one presented recently in [60]. The performances of our algorithm are of the same order as in [60].

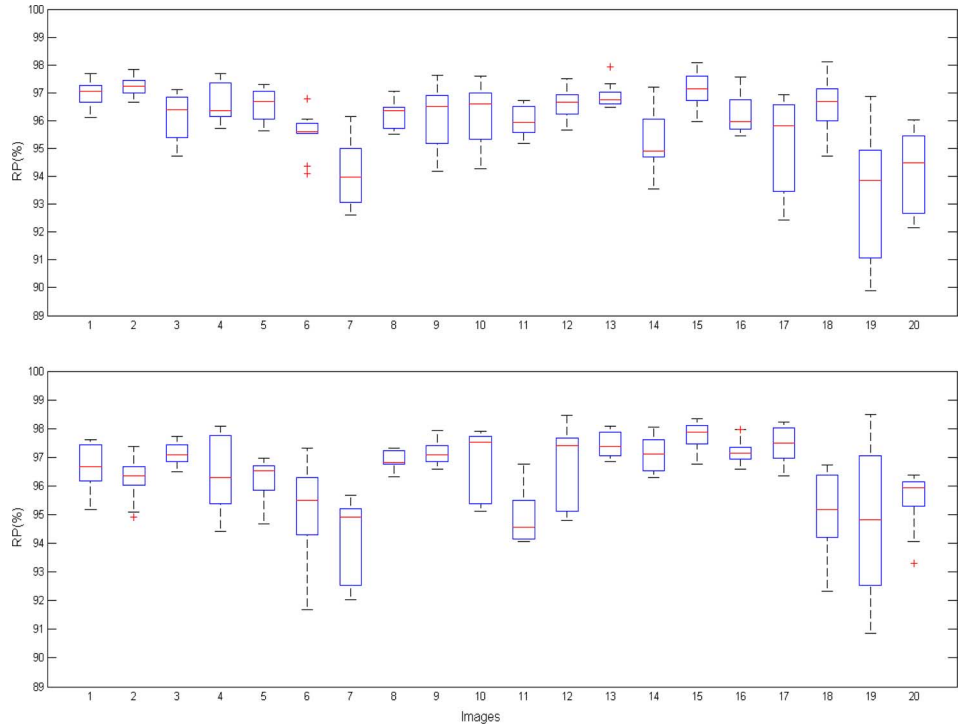

Fig. 8. Boxplots of the DSC (%) distance between all manual segmentations for the 20 images. (Top) Results of the first physician and (bottom) results of the second physician. The *x*-axis represents the image number.

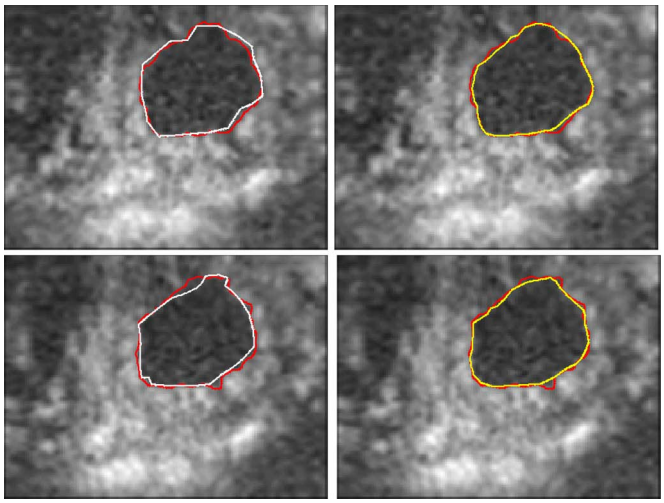

Fig. 9. Comparison of computer-generated segmentation (red) and the reference segmentation obtained from the manually delineated contours performed by the specialists. White in left column for the first specialist and yellow in right column for the second.

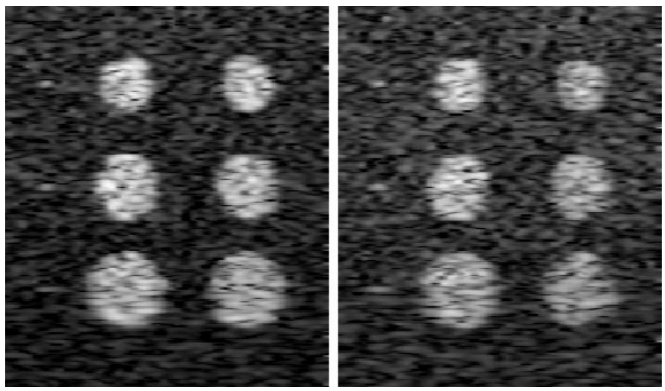

Fig. 10. Synthetic phantom. From left to right, high to low contrast circles. The three circles in each column, from top to bottom, have 17, 20, and 23 pixels radius, respectively.

The experiments on the simulated data also confirm our observations regarding the relative performances of the three compared methods. The results of the proposed PBLS and GAC + ML methods are better than those of GAC. Although, the GAC provides also acceptable results as it can be observed in Fig. 11. The PBLS segmentation provides the best results in terms of average performances and in terms of regularity as it has also the lower variances. An important observation is the large variance of the GAC + ML method. Our observation of its behavior suggests that it is mainly because of the simulated attenuation on some images that makes this variance increase. This reinforces our conclusion regarding the robustness of the proposed work relatively to other existing alternatives. Note, however, that recent works on region-based segmentation propose solutions for the segmentation of image with slow varying images statistics (see, e.g., [61] and [62]).

TABLE II
DSC (%) RESULTS OF THE TWO INTRAOBSERVERS AND INTEROBSERVER FOR TEN IMAGES

Images	1	2	3	4	5	6	7	8	9	10
Intraobserver 1	96.23	96.58	96.88	95.29	97.09	96.20	95.27	96.59	93.32	94.22
Intraobserver 2	96.74	96.71	97.43	97.07	97.78	97.22	97.41	95.07	94.74	95.48
Interobserver 1/2	87.61	89.27	97.17	96.96	97.13	95.96	87.61	87.24	93.30	92.82

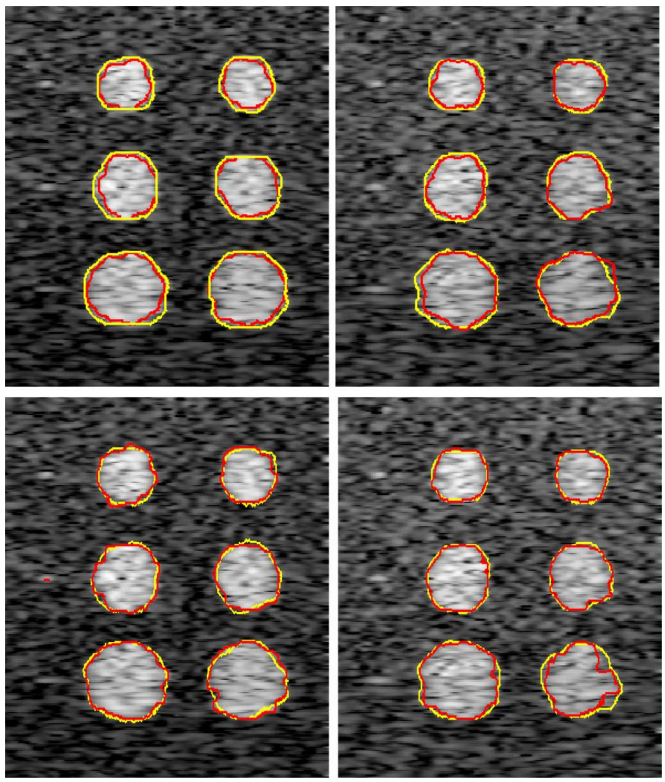

Fig. 11. Comparison of the PBLS segmentations (yellow) with the GAC segmentations (red, first line) and the GAC + ML segmentations (red, second line).

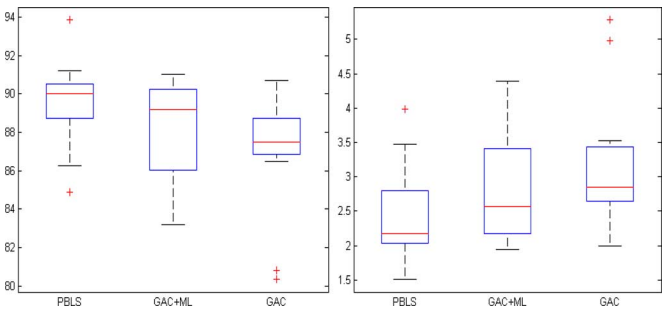

Fig. 12. Boxplot of the DSC (%) measure (left) and MAD distance (right) of the semiautomatic segmentation: PBLS, GAC + ML, and GAC.

VI. CONCLUSION

We have presented in this paper a new approach for the segmentation of the left ventricle in ultrasound images. In a level set framework, we integrate the use of a novel speed term based on local phase information and local orientation; both estimated using the monogenic signal. A key advantage of this approach is that it is more robust to intensity inhomogeneities.

The performance of the proposed PBLS segmentation is demonstrated on B-mode echocardiographic images and on realistic synthesized images. Quantitative results are shown, when compared against hand-outlined boundaries, and are of the same order as in the state of art. Experiments on synthetic data show, as expected, that the PBLS approach outperform the classical-intensity-based GAC and GAC + ML models. Although the quantitative evaluation was performed on a limited dataset, our experiments show that the proposed terms can favorably replace classical ones of the same nature. It is interesting to investigate the addition of more recent region terms, as in [61] and [62], at least at the beginning of the segmentation process, in order to improve the capture range of the method.

APPENDIX

PHASE-BASED ALIGNMENT TERM

The Laplacian term presented in [52], in its implicit forme, is given by

$$\phi_t = -\text{sign}(< \nabla\phi, \mathbf{V} >)\text{div}(\mathbf{V})|\nabla\phi| \tag{16}$$

where ϕ is a level set function and $\mathbf{V}$ is a vector field. The aim of our work is to build a Laplacian term based on a robust orientation estimation. Thus, we integrate the use of the phase vector Φ given in (4) as a vector field. The phase-based alignment term is then given by

$$\phi_t = -\text{sign}(< \nabla\phi, \Phi >)\text{div}(\Phi)|\nabla\phi| \tag{17}$$

$$= -\text{sign}(< \nabla\phi, \varphi \cdot \mathbf{r} >)\text{div}(\Phi)|\nabla\phi| \tag{18}$$

$$= -\text{sign}(\varphi\nabla\phi_{\mathbf{r}})\text{div}(\Phi)|\nabla\phi| \tag{19}$$

where $\nabla_{\mathbf{r}}$ is the gradient operator in the direction specified by $\mathbf{r}$. Notice that, because $\varphi \in [0, \pi]$, the sign of the product $\varphi\nabla\phi_{\mathbf{r}}$ depends only on the inner product between $\nabla\phi$ and the direction specified by $\mathbf{r}$. This leads to the following simplified formula:

$$\phi_t = -\text{sign}(\nabla\phi_{\mathbf{r}})\text{div}(P)|\nabla\phi|. \tag{20}$$

ACKNOWLEDGMENT

The authors would like to thank the anonymous reviewers for their helpful comments, and Dr. Mathiron and Dr. Levy for their help in the clinical evaluation of the data.

REFERENCES

[1] C. B. Burckhardt, "Speckle in ultrasound B-mode scans," *IEEE Trans. Sonics Ultrason.*, vol. SU-25, no. 1, pp. 1–6, Jan. 1978.
[2] R. F. Wagner, S. W. Smith, J. M. Sandrik, and H. Lopez, "Statistics of speckle in ultrasound B-scans," *IEEE Trans. Sonics Ultrason.*, vol. SU-30, no. 3, pp. 156–163, May 1983.
[3] P. M. Shankar, J. M. Reid, H. Ortega, C. W. Piccoli, and B. B. Goldberg, "Use of non-Rayleigh statistics for the identification of tumors in ultrasonic B-scans of the breast," *IEEE Trans. Med. Imag.*, vol. 12, no. 4, pp. 687–692, Dec. 1993.
[4] V. Dutt and J. F. Greenleaf, "Ultrasound echo envelope analysis using a homodyned K-distribution signal model," *Ultrason. Imag.*, vol. 16, no. 4, pp. 265–287, Oct. 1994.
[5] V. Dutt and J. F. Greenleaf, "Statistics of the log-compressed echo envelope," *J. Acous. Soc. Am.*, vol. 99, no. 6, pp. 3817–3825, Jun. 1996.
[6] P. M. Shankar, "A general statistical model for ultrasonic backscattering from tissues," *IEEE Trans. Ultrason., Ferroelectr., Freq. Control*, vol. 47, no. 3, pp. 727–737, May 2000.
[7] J. A. Noble and D. Boukerroui, "Ultrasound image segmentation: A survey," *IEEE Trans. Med. Imag.*, vol. 25, no. 8, pp. 987–1010, Jul. 2006.

[8] S. Nadarajah, "Statistical distributions of potential interest in ultrasound speckle analysis," *Phys. Med. Biol.*, vol. 52, pp. 213–227, 2007.

[9] D. A. N. Friedland, "Automatic ventricular cavity boundary detection from sequential ultrasound images using simulated annealing," *IEEE Trans. Med. Imag.*, vol. 8, no. 4, pp. 344–535, Dec. 1989.

[10] E. A. Ashton and K. J. Parker, "Multiple resolution bayesian segmentation of ultrasound images," *Ultrason. Imag.*, vol. 17, pp. 291–304, 1999.

[11] M. Mignotte, J. Meunier, and J.-C. Tardif, "Endocardial boundary estimation and tracking in echocardiographic images using deformable template and markov random fields," *Pattern Anal. Appl.*, vol. 4, no. 4, pp. 256–271, 2001.

[12] G. F. Xiao, M. Brady, J. A. Noble, and Y. Y. Zhang, "Segmentation of ultrasound B-mode images with intensity inhomogeneity correction," *IEEE Trans. Med. Imag.*, vol. 21, no. 1, pp. 48–57, Jan. 2002.

[13] D. Boukerroui, A. Baskurt, J. A. Noble, and O. Basset, "Segmentation of ultrasound images: multiresolution 2D and 3D algorithm based on global and local statistics," *Pattern Recogn. Lett.*, vol. 24, no. 4–5, pp. 779–790, 2003.

[14] A. Sarti, C. Corsi, E. Mazzini, and C. Lamberti, "Maximum likelihood segmentation of ultrasound images with rayleigh distribution," *IEEE Trans. Ultrason., Ferroelectr., Freq. Control*, vol. 52, no. 6, pp. 947–960, Jun. 2005.

[15] Z. Tao and H. Tagare, "Evaluation of four probability distribution models for speckle in clinical cardiac ultrasound images," *IEEE Trans. Med. Imag.*, vol. 25, no. 11, pp. 1483–1491, Nov. 2006.

[16] Y. Zhu, X. Papademetris, A. J. Sinusas, and J. S. Duncan, "A coupled deformable model for tracking myocardial borders from real-time echocardiography using an incompressibility constraint," *Med. Image Anal.*, vol. 14, pp. 429–448, 2010.

[17] T. Eltoft, "The rician inverse gaussian distribution: A new model for nonrayleigh signal amplitude statistics," *IEEE Trans. Image Process.*, vol. 14, no. 11, pp. 1722–1735, Nov. 2005.

[18] T. Eltoft, "Modeling the amplitude statistics of ultrasonic images," *IEEE Trans. Med. Imag.*, vol. 25, no. 2, pp. 1722–1735, Feb. 2006.

[19] Z. Tao and H. Tagare, "Tunneling descent level set segmentation of ultrasound images," in *Proc. Info. Med. Imag.*, 2005, pp. 750–761.

[20] Z. Tao and H. D. Tagare, "Tunneling descent for m.a.p. active contours in ultrasound segmentation," *Med. Image Anal.*, vol. 11, no. 3, pp. 266–281, 2007.

[21] M. Alemán-Flores, L. Álvarez, and V. Caselles, "Texture-oriented anisotropic filtering and geodesic active contours in breast tumor ultrasound segmentation," *J. Math. Imag. Vision*, vol. 28, no. 1, pp. 81–97, 2007.

[22] M. C. Morrone, J. Ross, D. C. Burr, and R. Owens, "Mach bands are phase dependent," *Nature*, vol. 324, no. 6094, pp. 250–253, Nov. 1986.

[23] M. C. Morrone and R. A. Owens, "Feature detection from local energy," *Pattern Recogn. Lett.*, vol. 6, no. 5, pp. 303–313, 1987.

[24] P. Kovesi, "Image features from phase congruency," *J. Comput. Vis. Res.*, vol. 1, no. 3, pp. 1–26, 1999.

[25] M. Mulet-Parada and J. A. Noble, "2D+T acoustic boundary detection in echocardiography," in *MICCAI*. London, U.K.: Springer-Verlag, 1998, pp. 806–813.

[26] M. Mulet-Parada and J. Noble, "2D+T acoustic boundary detection in echocardiography," *Med. Image Anal.*, vol. 4, no. 1, pp. 21–30, 2000.

[27] I. Hacihaliloglu, R. Abugharbieh, A. Hodgson, and R. Rohling, "Bone segmentation and fracture detection in ultrasound using 3d local phase features," in *MICCAI*, Berlin, Heidelberg: Springer-Verlag, 2008, pp. 287–295.

[28] G. Läthén, J. Jonasson, and M. Borga, "Phase based level set segmentation of blood vessels," in *Proc. 19th ICPR*, Tampa, FL: IAPR, Dec.2008, pp. 1–4.

[29] R. Ali, M. J. Gooding, M. Christlieb, and J. M. Brady, "Phase-based segmenation of cells with brightfield microscopy," in *Proc. IEEE Symp. Biomed. Imag.*, 2007, pp. 57–60.

[30] D. Boukerroui, J. A. Noble, M. C. Robini, and J. Brady, "Enhancement of contrast regions in sub-optimal ultrasound images with application to echocardiography," *Ultrasound Med. Biol.*, vol. 27, no. 12, pp. 1583–1594, 2001.

[31] M. Mellor and M. Brady, "Phase mutual information as a similarity measure for registration," *Med. Image Anal.*, vol. 9, no. 4, pp. 330–343, 2005.

[32] V. Grau, H. Becher, and J. A. Noble, "Registration of multiview real-time 3-D echocardiographic sequences," *IEEE Trans. Med. Imag.*, vol. 26, no. 9, pp. 1154–1165, Sep. 2007.

[33] V. Murray, S. E. Murillo, M. S. Pattichis, C. P. Loizou, C. S. Pattichis, E. Kyriacou, and A. Nicolaides, "An AM-FM model for motion estimation in atherosclerotic plaque videos," in *Proc. Asilomar Conf. Signals, Syst. Compt.*, Nov. 2007, pp. 746–750.

[34] V. Murray, E. S. Barriga, P. Soliz, and M. S. Pattichis, "Survey of AM-FM methods for applications on medical imaging," in *Proc. Ibero-American Conf. Trends Eng. Edu. Collab.*, Albuquerque, NM, Oct. 2009.

[35] I. Kokkinos, G. Evangelopoulos, and P. Maragos, "Texture analysis and segmentation using modulation features, generative models, and weighted curve evolution," *IEEE Trans. Pattern Anal. Mach. Intell.*, vol. 31, no. 1, pp. 142–157, Jan. 2009.

[36] M. Unser, D. Sage, and D. V. D. Ville, "Multiresolution monogenic signal analysis using the riesz-laplace wavelet transform," *IEEE Trans. Image Process.*, vol. 18, no. 11, pp. 2402–2418, Nov. 2009.

[37] M. S. Pattichis and A. C. Bovik, "Analyzing image structure by multidimensional frequency modulation," *IEEE Trans. Pattern Anal. Mach. Intell.*, vol. 29, no. 5, pp. 753–766, May 2007.

[38] V. Murray, P. Rodriguez, and M. S. Pattichis, "Multiscale AM-FM demodulation and image reconstruction methods with improved accuracy," *IEEE Trans. Image Process.*, vol. 19, no. 5, pp. 1138–152, May 2010.

[39] D. J. Fleet, D. J. Fleet, A. D. Jepson, A. D. Jepson, M. R. M. Jenkin, and M. R. M. Jenkin, "Phase-based disparity measurement," *CVGIP: Image Understand.*, vol. 53, no. 2, pp. 198–210, 1991.

[40] J. Zhou, Y. Xu, and X. Yang, "Quaternion wavelet phase based stereo matching for uncalibrated images," *Pattern Recogn. Lett.*, vol. 28, no. 12, pp. 1509–1522, 2007.

[41] D. Zang, L. Wietzke, C. Schmaltz, and G. Sommer, "Dense optical flow estimation from the monogenic curvature tensor," in *SSVM*, 2007, pp. 239–250.

[42] A. Wong, "Fast communication: Adaptive bilateral filtering of image signals using local phase characteristics," *Signal Process.*, vol. 88, no. 6, pp. 1615–1619, 2008.

[43] P. Kovesi, "Phase congruency detects corners and edges," in *Proc. Aust. Pattern Recog. Soc. Conf.: DICTA*, 2003, pp. 309–318.

[44] M. Felsberg and G. Sommer, "A new extension of linear signal processing for estimating local properties and detecting features," in *Proc. 22nd DAGM Symp. Mustererkennung*, 2000, pp. 195–202.

[45] M. Felsberg and G. Sommer, "The monogenic signal," *IEEE Trans. Signal Process.*, vol. 49, no. 12, pp. 3136–3144, Dec. 2001.

[46] M. Felsberg and G. Sommer, "The monogenic scale-space: A unifying approach to phase-based image processing in scale-space," *J. Math. Imag. Vis.*, vol. 21, no. 1, pp. 5–26, 2004.

[47] A. Belaid, D. Boukerroui, Y. Maingourd, and J.-F. Lerallut, "Phase based level set segmentation of ultrasound images," in *Proc. 9th IEEE Int. Conf. Inf. Tech. App. Biomed.*, 2009.

[48] A. V. Oppenheim and J. S. Lim, "The importance of phase in signals," *Proc. IEEE*, vol. 69, no. 5, pp. 529–541, May 1981.

[49] G. H. Granlund and H. Knutsson, *Signal Processing for Computer Vision*. Norwell, MA: Kluwer Publ., 1995.

[50] D. Boukerroui, J. A. Noble, and M. Brady, "On the choice of band-pass quadrature filters," *J. Math. Imag. Vision*, vol. 21, no. 1, pp. 53–80, 2004.

[51] D. Boukerroui, J. A. Noble, and M. Brady, *Frontiers in Robotics Research*, M. A. Denket Ed. New York: Nova Publ., 2006, ch. On the Selection of Band-Pass Quadrature Filters, pp. 67–111..

[52] R. Kimmel and A. M. Bruckstein, "Regularized laplacian zero crossings as optimal edge integrators," *Int. J. Comp. Vision*, vol. 53, no. 3, pp. 225–243, 2003.

[53] V. Caselles, R. Kimmel, and G. Sapiro, *Handbook of Image and Video Processing*, A. C. Bovik Ed., 2nd revised ed. New York: Academic, 2005, ch. Geometric active contours for image segmentation, pp. 613–629.

[54] V. Caselles, R. Kimmel, and G. Sapiro, "Geodesic active contours," *Int. J. Comp. Vision*, vol. 22, no. 1, pp. 61–79, 1997.

[55] R. Kimmel, "Fast edge integration," in *Geometric Level Set Methods in Imaging, Vision, and Graphics*. S. Osher and N. Paragios, Eds. New York: Springer, 2003, pp. 59–77.

[56] L. R. Dice, "Measures of the amount of ecologic association between species," *Ecology*, vol. 26, no. 3, pp. 297–302, 1945.

[57] V. Chalana, D. T. Linker, D. R. Haynor, and Y. Kim, "A multiple active contour model for cardiac boundary detection on echocardiographic sequences," *IEEE Trans. Med. Imag.*, vol. 15, no. 3, pp. 290–298, Jun. 1996.

[58] J. A. Jensen and N. B. Svendsen, "Calculation of pressure fields from arbitrarily shaped, apodized, and excited ultrasound transducers," *IEEE Trans. Ultrason., Ferroelec., Freq. Contr.*, vol. 39, no. 2, pp. 262–267, Mar. 1992.

[59] J. A. Jensen, "Field: A program for simulating ultrasound systems," in *Proc. 10th Nordic-Baltic Conf. Biomed. Imag.*, 1996, vol. 34, pp. 351–353.
[60] M. Alemán-Flores, L. Álvarez-León, and V. Caselles, "Texture-oriented anisotropic filtering and geodesic active contours in breast tumor ultrasound segmentation," *J. Math. Imag. Vision*, vol. 28, no. 1, pp. 81–97, 2007.
[61] S. Lankton and A. Tannenbaum, "Localizing region-based active contours," *IEEE Trans. Image Process.*, vol. 17, no. 11, pp. 2029–2039, Nov. 2008.
[62] T. Brox and D. Cremers, "On local region models and a statistical interpretation of the piecewise smooth mumford-shah functional," *Int. J. Comp. Vision*, vol. 84, no. 2, pp. 184–193, 2009.

Ahror Belaid received the M.S. degree in operation research from University of Abderrahmane Mira, Bejaia, Algeria. He is currently working toward the Ph.D. degree in the Department of Information Processing Engineering, Compiègne University of Technology, Compiègne, France.

His current research interests include the phase-based ultrasound images segmentation.

Djamal Boukerroui was born in Bejaïa, Algeria, in 1972. He received the B.S. degree in 1990 and the M.S. degree in electronics in July 1995 from Ecole Nationale Polytechnique of Algiers, Algeria, and the Ph.D degree in image processing from CREATIS Laboratory, INSA, Lyon, France, in 2000.

From March 2000 to August 2002, he was a Research Assistant at the Medical Vision Laboratory, Department of Engineering Science, University of Oxford, where he was involved on the analysis of echocardiographic image sequences. In September 2002, he joined the Department of Information Processing Engineering, Compiègne University of Technology, Compiègne, France as Maître de Conffences, where he is also a Member of HEUDIASYC [research unit associated with CNRS #6599)]. His current research interests include low-level image processing, and specifically, its application in ultrasound image analysis.

Y. Maingourd's photograph and biography not available at the time of publication.

Jean-Francois Lerallut (SM'06) received the M.S. degree in electronics from Ecole Spéciale de Mécanique et d' Electricité, Paris, France, in 1976, and the Ph.D. degree from University of Technology of Compiegne (UTC), Compiegne, France, in 1979.

From 1979 to 2005, he was in the Department of Biomedical Engineering, UTC, where he is currently a Professor and also with the research unit HEUDIASYC associated with CNRS #6599.

Prof. Lerallut served in program committees and organizing committees for many international conferences. He is currently involved in projects on medical image processing.